

Crystallization of lysozyme with (R)-, (S)- and (RS)-2-methyl-2,4-pentanediol

Mark Stauber^{ab1}, Jean Jakoncic^c, Jacob Berger^{ab2}, Jerome M. Karp^{ab3},
Ariel Axelbaum^{ab}, Dahniel Sastow^{ab}, Sergey V. Buldyrev^a, Bruce J.
Hrnjez^d and Neer Asherie^{ab*}

^aDepartment of Physics, Yeshiva University, 2495 Amsterdam Avenue, NY, NY,
10033-3312, USA,

^bDepartment of Biology, Yeshiva University, 2495 Amsterdam Avenue, NY, NY,
10033-3312, USA,

^cNational Synchrotron Light Source, Brookhaven National Laboratory, Building
725D, Upton, NY, 11973-5000, USA, and

^dCollegiate School, 260 West 78th Street, New York, NY, 10024-6559, USA
Correspondence email: asherie@yu.edu

¹Present address: Mechanical Engineering Department, Stanford University, 440
Escondido Mall, Stanford, CA 94305-3030, USA

²Present address: Department of Materials Science and Engineering, University of
Pennsylvania, 3231 Walnut Street, Philadelphia, PA 19104-6272, USA

³Present Address: Albert Einstein College of Medicine, Yeshiva University, 1300
Morris Park Avenue, Bronx, NY 10461-1900, USA

Submitted to Crystallographica

March 2015

National Synchrotron Light Source II

Brookhaven National Laboratory

**U.S. Department of Energy
DOE – Office of Science**

Notice: This manuscript has been co-authored by employees of Brookhaven Science Associates, LLC under Contract No. DE-SC0012704 with the U.S. Department of Energy. The publisher by accepting the manuscript for publication acknowledges that the United States Government retains a non-exclusive, paid-up, irrevocable, worldwide license to publish or reproduce the published form of this manuscript, or allow others to do so, for United States Government purposes.

DISCLAIMER

This report was prepared as an account of work sponsored by an agency of the United States Government. Neither the United States Government nor any agency thereof, nor any of their employees, nor any of their contractors, subcontractors, or their employees, makes any warranty, express or implied, or assumes any legal liability or responsibility for the accuracy, completeness, or any third party's use or the results of such use of any information, apparatus, product, or process disclosed, or represents that its use would not infringe privately owned rights. Reference herein to any specific commercial product, process, or service by trade name, trademark, manufacturer, or otherwise, does not necessarily constitute or imply its endorsement, recommendation, or favoring by the United States Government or any agency thereof or its contractors or subcontractors. The views and opinions of authors expressed herein do not necessarily state or reflect those of the United States Government or any agency thereof.

Crystallization of lysozyme with (*R*)-, (*S*)- and (*RS*)-2-methyl-2,4-pentanediol

Mark Stauber^{ab1}, Jean Jakoncic^c, Jacob Berger^{ab2}, Jerome M. Karp^{ab3}, Ariel Axelbaum^{ab}, Dahniel Sastow^{ab}, Sergey V. Buldyrev^a, Bruce J. Hrncic^d and Neer Asherie^{ab*}

^aDepartment of Physics, Yeshiva University, 2495 Amsterdam Avenue, New York, NY, 10033-3312, USA, ^bDepartment of Biology, Yeshiva University, 2495 Amsterdam Avenue, New York, NY, 10033-3312, USA, ^cNational Synchrotron Light Source, Brookhaven National Laboratory, Building 725D, Upton, NY, 11973-5000, USA, and ^dCollegiate School, 260 West 78th Street, New York, NY, 10024-6559, USA

Correspondence email: asherie@yu.edu

¹ Present address: Mechanical Engineering Department, Stanford University, 440 Escondido Mall, Stanford, CA 94305-3030, USA

² Present address: Department of Materials Science and Engineering, University of Pennsylvania, 3231 Walnut Street, Philadelphia, PA 19104-6272, USA

³ Present Address: Albert Einstein College of Medicine, Yeshiva University, 1300 Morris Park Avenue, Bronx, NY 10461-1900, USA

Keywords: MPD; crystallization additive; precipitant; high-resolution protein structures; chirality.

Synopsis

Crystallization of lysozyme with (*R*)-2-methyl-2,4-pentanediol produces more ordered crystals and a higher resolution protein structure than crystallization with (*S*)-2-methyl-2,4-pentanediol. The results suggest that chiral interactions with chiral additives are important in protein crystal formation.

Abstract

Chiral control of crystallization has ample precedent in the small-molecule world, but relatively little is known about the role of chirality in protein crystallization. In this study, lysozyme was crystallized in the presence of the chiral additive 2-methyl-2,4-pentanediol (MPD), separately using the *R* and *S* enantiomers as well as the racemic *RS* mixture. Crystals grown with (*R*)-MPD had the most order and

produced the highest resolution protein structures. This result is consistent with the observation that for (*R*)- and (*RS*)-MPD, the crystal contacts are made by (*R*)-MPD demonstrating that there is preferential interaction between lysozyme and this enantiomer. These findings suggest that chiral interactions are important in protein crystallization.

1. Introduction

Proteins are difficult to crystallize. According to the most recently available statistics from the Structural Biology Knowledgebase (Gabanyi *et al.*, 2011), fewer than one in eight purified proteins produce diffraction-quality crystals. Furthermore, this success rate has been decreasing over the past decade (Chayen, 2002, 2004; Chayen & Saridakis, 2008); one explanation offered is that the proteins which are easy to crystallize were tackled first (Pusey *et al.*, 2005).

A protein will crystallize when the solution conditions are thermodynamically and kinetically favorable (Candoni *et al.*, 2012). As there is currently no way to predict these favorable conditions, protein crystallization remains essentially a brute-force endeavor; many different conditions are examined in the hope that at least one of them will produce crystals (Chan *et al.*, 2013; Wilson & DeLucas, 2014). One common way to alter the solution conditions is through the use of additives. These additives are typically salts, small organic molecules, and polymers (Dumetz *et al.*, 2009; McPherson *et al.*, 2011), though other additives have been used, such as silicon-based surfaces that promote nucleation (Chayen *et al.*, 2001; Ghatak & Ghatak, 2011; Tsekova *et al.*, 2012).

Much has been done to understand the role of protein-additive interactions in crystal formation (McPherson, 1999). While the detailed mechanisms through which additives promote protein crystallization are often not known, a few general features of protein-additive interactions are understood. For example, additives can form favorable crystal contacts leading to a stable and highly ordered crystalline arrangement of proteins (McPherson *et al.*, 2011).

We are investigating an aspect of protein-additive interactions that is relatively unexplored in the context of protein crystallization: chirality. Chiral control of crystallization has ample precedent in the small-molecule world (Addadi *et al.*, 1982; Amharar *et al.*, 2012; Blackmond, 2011; Brittain, 2013; Eicke *et al.*, 2013; Gou *et al.*, 2012; Levilain *et al.*, 2012; Lorenz & Seidel-Morgenstern, 2014), but most of the work on chiral interactions between proteins and additives has focused on how such interactions control protein function (Brooks *et al.*, 2011). Typically, when a protein binds a small, chiral molecule, it interacts differently with one enantiomer than the other because the protein itself is chiral. In principle, such chiral interactions may affect not only protein function but also protein phase behaviour, including crystallization.

Our previous work on thaumatin and sodium tartrate demonstrated that the chirality of the additive has a substantial effect on the habit, packing, solubility and growth of protein crystals (Asherie,

Ginsberg, Blass, *et al.*, 2008; Asherie, Ginsberg, Greenbaum, *et al.*, 2008; Asherie *et al.*, 2009). Furthermore, by working with enantiomerically pure additives, we were able to determine the highest resolution (0.94 Å) thaumatin structure currently available (Asherie *et al.*, 2009).

To examine the generality of our findings, we are studying other pairs of proteins and chiral precipitants. Here we discuss our results for the crystallization of lysozyme with 2-methyl-2,4-pentanediol (MPD; C₆H₁₄O₂). We chose this protein-precipitant pair for three reasons. First, lysozyme is the most widely examined protein in crystallization and structural analysis studies (Chayen & Saridakis, 2001; Liang *et al.*, 2013; Magay & Yoon, 2011; Tu *et al.*, 2014). Second, MPD is a chiral molecule that is one of the most common additives in protein crystallization (Anand *et al.*, 2002), though it has been used exclusively as the racemate. Third, lysozyme has been previously crystallized with (*RS*)-MPD, but the results of these investigations are contradictory: Weiss finds only (*R*)-MPD in the crystal (Weiss *et al.*, 2000), whereas Michaux finds only (*S*)-MPD (Michaux *et al.*, 2008).

In the current study, we crystallized lysozyme using the individual *R* and *S* enantiomers of MPD separately as well as the racemate, and determined the x-ray structures of the resultant crystals. We determined also the x-ray structure of lysozyme crystals grown without MPD. All structures were obtained to high resolution (1.25 Å or better), allowing for a detailed comparison of the protein structures and—in principle—an unambiguous assignment of the absolute configuration (*R* or *S*) of the MPD molecules. This assignment, however, is complicated by the fact that the MPD molecule can adopt different conformations (Anand *et al.*, 2002). We therefore performed a detailed conformational analysis of MPD using quantum chemical (QC) calculations and molecular dynamics (MD) simulations. Consequently, we were able to use the stable conformer that likely dominates the relative conformer population in our analysis of the protein crystal structures. Ambiguity in the analysis is thereby diminished.

We find that crystals grown with (*R*)-MPD had the least disorder (as measured by the mosaicity and B-factor) and produced the highest resolution protein structures. This finding is consistent with the observation that co-crystallization with either (*R*)- or (*RS*)-MPD gives crystal contacts made exclusively by (*R*)-MPD, demonstrating that there is preferential interaction between lysozyme and this enantiomer. These results support the hypothesis that chiral interactions may be important in protein crystallization with chiral additives.

2. Materials and methods

2.1. Materials

Lysozyme (cat. no. 2933, lot no. 36P9210) was purchased from Worthington Biochemical Corporation (Lakewood, NJ). (*R*)-MPD and (*S*)-MPD were synthesized by Reuter Chemische

Apparatebau KG (Freiburg, Germany). (*RS*)-MPD (cat. no. 68340, lot no. 1345630) was purchased from Sigma-Aldrich (St. Louis, MO). Tris base (cat. no. BP512-500), sodium azide (cat. no. S227I-500), and hydrochloric acid (cat. no. A144S-500) were purchased from Fisher Scientific (Pittsburgh, PA). All materials were used without further purification. The purity of the protein and the chemical and enantiomeric purity of (*R*)-, (*S*)- and (*RS*)-MPD were determined as described in the Supplementary Material. Deionized water was obtained from an Integral 3 deionization system (Millipore, Billerica, MA). Solutions were filtered through a Nalgene disposable 0.22 μm filter unit (Nalge Nunc International, Rochester, NY) prior to use.

Concentration measurements were carried out by UV-Vis extinction spectroscopy on a Beckman-Coulter DU800 spectrophotometer. The extinction coefficient of lysozyme at 280 nm was taken to be $E^{0.1\%} = 2.64 \text{ mg ml}^{-1} \text{ cm}^{-1}$ (Aune & Tanford, 1969). Conductivity and pH measurements were performed using an Orion 4-Star conductivity and pH meter with a DuraProbe conductivity cell and a RossSure-Flow pH electrode (Thermo Fisher Scientific, Waltham, MA).

2.2. Protein crystallization

Lysozyme was dissolved in 200 mM Tris (titrated to pH 8.0 with HCl; $\sigma = 9.90 \text{ mS/cm}$), washed three times in the same buffer in an Amicon Ultra-4 centrifugal filter device with a 3 kDa molecular weight cutoff (Millipore, Billerica, MA) and then concentrated to approximately 35 mg/ml. Crystals were grown using the vapor diffusion hanging drop method in the EasyXtal 15-Well Tool (cat no. 132006; Qiagen, Valencia, CA). Drops were made by mixing 10 μl of the protein solution with 10 μl of the reservoir solution. This mixture was vortexed briefly and then three 5 μl drops were dispensed on the crystallization supports. The reservoir solutions (300 μl) were 60% (v/v) (*R*)-, (*S*)- or (*RS*)-MPD in water. A control experiment with only water in the reservoir was also carried out. The crystallization trays were left at $4.0 \pm 0.5 \text{ }^\circ\text{C}$ and inspected periodically by bright field microscopy with an AxiImager A1m microscope (Carl Zeiss, Göttingen, Germany). Crystals of roughly 200 μm in size grew in about 5 days with MPD (Supplementary Figure S1); crystals of similar size took about two weeks to grow in the control. Crystals were harvested with mounted cryoloops (Hampton Research, Aliso Viejo, CA). No cryoprotectant was used, except for crystals grown in the control, which were dipped in Paratone N (Hampton Research, Aliso Viejo, CA) immediately before the diffraction measurements.

2.3. Data collection, refinement and structural analysis

All X-ray diffraction data were recorded at beamline X6A (Brookhaven National Laboratory, National Synchrotron Light Source, Upton, NY, USA) between 13.5 and 15.1 keV. All data were

recorded at 100 K using an ADSC Q270 CCD detector (Poway, CA, USA). Data were indexed, integrated and scaled in HKL 2000 (Otwinowski & Minor, 1997). Lysozyme crystal structures were solved by molecular replacement using MOLREP (Vagin & Teplyakov, 1997) and the model from the PDB entry 1IEE (Sauter *et al.*, 2001). Each model was refined by restrained maximum-likelihood refinement with REFMAC (Murshudov *et al.*, 1997; Winn *et al.*, 2011) with individual anisotropic temperature factors and manual building performed in Coot (Emsley *et al.*, 2010). After the final refinement, stereochemistry of the structures was assessed with PROCHECK (Laskowski *et al.*, 1993). All figures were prepared with PyMOL (The PyMOL Molecular Graphics System, Schrödinger, LLC).

2.4. Quantum chemical calculations and molecular dynamics simulations

Ab initio electronic structure calculations for the nine (*R*)-MPD conformers **1** - **3** (see Fig. 2) were performed with Gaussian09 (Frisch *et al.*, 2009). Stationary points were located on the local potential surfaces for these nine conformers at a modest level of quantum chemical theory, using the second-order Møller-Plesset perturbation (MP2) method (Møller & Plesset, 1934) and the 6-311++G(d,p) medium-sized basis (Clark *et al.*, 1983) set for C, H, and O. Program package defaults, including criteria for wave function convergence and locations of stationary points on potential surfaces, were used. The nine initial input structures were the result of a qualitative conformational analysis of the all-staggered conformational possibilities for (*R*)-MPD. Conformer **1a** was assumed to be intramolecularly H-bonded; we were able to focus on a single conformer because the geometry optimized energies of different intramolecularly H-bonded rotamers about C-O bonds differed by less than 1 kJ mol⁻¹. As expected, inversion of configuration at C4 to give (*S*)-MPD gave identical computational results.

We examined the effect of water solvation on the relative conformer energies at the same level of quantum chemical theory, incorporating the default integral equation formalism variant (IEF) within the polarizable continuum model (PCM) for placing a solute in a cavity within the solvent reaction field (SCRF) (Tomasi *et al.*, 2005).

Molecular dynamics simulations of both (*R*)-MPD and (*S*)-MPD were performed using GROMACS v.4.0.5 (Hess *et al.*, 2008). The initial coordinates for (*R*)- and (*S*)-MPD were taken from PDB entries 4B4E and 4B4I, respectively, with hydrogen atoms added using the pdb2gmx utility of GROMACS. Simulations were run *in vacuo* with one molecule of either (*R*)- or (*S*)-MPD placed in a cubic box of length 3.0 nm with periodic boundary conditions. Since MPD has no net charge, no counterions were added. The topology files were constructed using parameters for OPLS-AA atom types (Jorgensen *et al.*, 1996; Jorgensen & Tiradorives, 1988). The properties of the atoms used in the topology file for both are shown in the Supplementary Table S1.

The OPLS-AA all-atom force field was used in running simulations. Each simulation box was subjected to energy minimization using the steepest descent method. Simulations were run using the NVT ensemble, and the temperature was held constant at 300 or 370 K using the V-rescale thermostat (Bussi *et al.*, 2009) with a coupling constant of 0.1. Electrostatic interactions were treated using the particle mesh Ewald algorithm (Essmann *et al.*, 1995) using electrostatic, van der Waals and neighbor list cutoffs of 0.9 nm. The SHAKE constraint algorithm (Ryckaert *et al.*, 1977) was used to constrain all bonds with a tolerance of 0.0002. Simulations were run for 100 ns, using 1 fs time steps and saving coordinates and energies every 1 ps. The first 10 ns of each simulation were considered equilibration time and not used in subsequent analysis.

Annealing simulations were run with (*R*)-MPD *in vacuo*. The systems were prepared as above. In each of 100 simulations, the initial velocities were independently randomly generated. The initial temperature was 370 K and the simulation was run for 200 ps. Over every subsequent 200 ps, the temperature was decreased linearly with time by 5 K. Thus, 14.6 ns after the beginning the simulations, the temperature reached 5 K. During the next 200 ps, the temperature was decreased linearly with time to 0.1 K. The simulation continued at this temperature until it had run for a total of 20 ns.

Trajectory analysis was performed with the GROMACS utilities package. For clarity, we report torsion angles in the range 0° to 360° instead of the customary -180° to 180° (torsion angles greater than 180° can be converted to the usual negative torsion angles by subtracting 360°).

2.5. Database analysis

MPD conformations were extracted from the RCSB Protein Data Bank (PDB) [www.pdb.org; (Berman *et al.*, 2000).] and the Cambridge Structural Database (CSD) (Allen, 2002). The PDB was searched using the chemical IDs for either (*R*)-MPD (MRD) or (*S*)-MPD (MPD) together with two additional requirements: x-ray resolution between 0 and 1.5 Å and sequence homology of less than 90% with other macromolecules. This search yielded 49 protein structure hits for MRD and 89 protein structure hits for MPD. Some of these hits contained both enantiomers yielding 117 unique protein structures with (*R*)- or (*S*)-MPD. (We note that numerous protein structures had more than one (*R*)- or (*S*)-MPD molecule associated with them.) These molecules were inspected using Coot (Emsley *et al.*, 2010) with the structure and electron density maps ($2F_o - F_c$ and $F_o - F_c$) downloaded through the Uppsala Electron Density Server (Kleywegt *et al.*, 2004). Hits that had no density or no structure factor were discarded. The quality of the electron density map, the local hydrogen bonding and the atomic B-factors of the molecules were used to check whether the assigned model (*R*)- or (*S*)-MPD structure was acceptable as is, i.e., whether the enantiomer and conformer selected were supported by the data. Acceptable structures were kept, while the unacceptable ones were either discarded (because

the torsion angles of the molecule could not be determined unambiguously) or reassigned to achieve a better agreement between the model and the electron density. The torsion angles of the acceptable and reassigned structures were measured using the built-in function of Coot. In total, 221 molecules were retained: 109 were (*R*)-MPD and 112 were (*S*)-MPD.

The CSD was searched with ConQuest (Bruno *et al.*, 2002) using the chemical formula of MPD (C₆H₁₄O₂). The resulting 28 hits were inspected and only the 7 hits that corresponded to 2-methyl-2,4-pentanediol were retained (reference codes: BACXIM10, FALDUS, KOFPAW, NIRQIO, NOSVOG, PIVYEZ and TECYIJ). The hits, some of which contained multiple molecules of both enantiomers, were examined using Mercury (Bruno *et al.*, 2002). Since no structure factor information was available, the assigned model (*R*)-MPD or (*S*)-MPD structures were accepted as is, unless the local hydrogen bonding suggested that the structure be reassigned. The torsion angles of the acceptable and reassigned structures were measured using the built-in function of Mercury. In total, 10 molecules were retained: 3 were (*R*)-MPD and 7 were (*S*)-MPD.

3. Results and discussion

3.1. Protein and precipitant purity

Protein purity is a crucial factor in crystallization (McPherson, 1999). Indeed, the deleterious effect of impurities on the crystallization of lysozyme has been studied extensively (Dold *et al.*, 2006; Judge *et al.*, 1998; Lorber *et al.*, 1993; Parmar *et al.*, 2007; Thomas *et al.*, 1996). We chose to work with lysozyme from Worthington Biochemical Corporation because it has been shown to produce high-quality crystals (Parmar *et al.*, 2007). Our characterization of the protein by size-exclusion and cation-exchange high-performance chromatography, quasielastic light scattering and electrospray ionization mass spectroscopy confirms its high purity (Supplementary Figs. S2-S3 and Table S2).

For the precipitant, both chemical and enantiomeric purity must be controlled. We purchased (*RS*)-MPD from Sigma-Aldrich, but decided against using the commercially available (*R*)-MPD from the same manufacturer (cat no. 252840) because of its lower chemical purity and limited information about its enantiomeric purity (only the specific rotation is given). For (*S*)-MPD, a commercial supplier was not an option. To our knowledge, this enantiomer is not available as a common chemical.

We therefore commissioned the custom syntheses of (*R*)-MPD and (*S*)-MPD by Reuter Chemische Apparatebau KG (the structure of the two enantiomers and associated nomenclature are shown in Fig. 1). Since (*S*)-MPD has not been characterized previously and only partial information is available for (*R*)-MPD, we analyzed these enantiomers and the racemate (*RS*)-MPD by ¹H and ¹³C NMR, tandem mass spectrometry and optical activity (Supplementary Figs. S4-S9 and Tables S3-S4). For

completeness, we also provide the gas chromatography results of (*R*)-MPD and (*S*)-MPD that were given to us by the manufacturer (Supplementary Figs. S10-S11). These results confirm the chemical identity of the molecules synthesized and demonstrate their high chemical and enantiomeric purity; the key results are summarized in Table 1.

3.2. MPD conformation

An important step in the analysis of the x-ray diffraction data is the proper assignment of any MPD molecules present in the crystal structure. This assignment involves selecting the enantiomer(s) and conformer(s) of the molecule that best fit the electron density. For the experiments with pure (*R*)- or (*S*)-MPD, there is only one enantiomer to choose, but for crystallization with (*RS*)-MPD, the selection is less straightforward.

If the electron density map is of sufficiently high quality, it is possible to distinguish the two enantiomers by inspecting the shape of the map, even though the hydrogen atom on the chiral center C4 (Fig. 1) is not visible in the x-ray data. An example is the (*R*)-MPD molecule found near F34 by Weiss *et al.* in the structure of lysozyme (PDB code 1DPW) crystallized with (*RS*)-MPD (Weiss *et al.*, 2000). If the shape of the map is inconclusive, knowledge of the most likely conformer can be helpful in selecting the appropriate enantiomer.

Since hydrogen atoms contribute little to the electron density, the conformation of MPD as obtained from the electron density map is completely determined by the torsion angles (ψ_1 , ψ_2), which are defined by the carbon atoms C1-C2-C3-C4 and C2-C3-C4-C5, respectively (Fig. 1). Furthermore, for an isolated molecule, the stable conformers of one enantiomer will be mirror images of the other. Energetic considerations suggest that the expected values of these angles for an isolated (*R*)-MPD molecule are approximately (180° , 180°). This conformation (shown in Fig. 1) allows for the formation of an intramolecular hydrogen bond—the distance between O2 and O4 atoms is 2.8 Å—and corresponds to a favorable arrangement of the C1-C2-C3-C4-C5 backbone (Salam & Deleuze, 2002). To verify these considerations, we carried out both quantum chemical calculations and molecular dynamics simulations on MPD.

We performed quantum chemical (QC) calculations to determine the relative energies of nine conformers of (*R*)-MPD shown schematically in Fig. 2. These all-staggered conformers were chosen as the initial configurations for geometry optimization; each of these is likely to be close to a local minimum on the conformational potential energy surface (Mo, 2010). The relative energies of the optimized geometries for the nine conformers are listed in Table 2 (see also Supplementary Table S5). As expected, **1a** is the most stable conformer *in vacuo* and the torsion angles of the final, geometry-optimized structure are (177° , 173°), close to the qualitatively predicted (180° , 180°). Furthermore, there is a significant gap in energy between **1a** and the next most stable conformer, **3a** (Fig. 2).

Conformer **3a** cannot accommodate an intramolecular hydrogen bond because O2 and O4 are too far apart (3.9 Å). Indeed, the energy difference (12.4 kJ mol⁻¹) between **3a** and **1a** falls within the range of hydrogen bond energies (9.2–24.3 kJ mol⁻¹) calculated for other alkanediols (Mandado *et al.*, 2006). Finally, we verified for conformer **1a** that the (*R*)- and (*S*)-MPD enantiomers have identical energies.

Since our protein crystals form in the presence of solvent, we also calculated the relative energies of the conformers using a polarizable continuum model of water (Scalmani & Frisch, 2010). While the exact values of the relative energies are slightly different from those found *in vacuo*, the ranking of conformers in terms of stability is the same (Table 2). In particular, the most stable conformer is **1a** and there is an energy difference corresponding to the loss of the intramolecular hydrogen bond for the next most stable conformer **3a**.

The results above indicate that **1a** is the most stable conformer in a variety of environments. However, the actual population of conformers in any given environment will be determined not solely by energetic factors, but by entropic ones as well, i.e., by the relative free energies. To determine the relative free energies of MPD, we performed MD simulations *in vacuo* at 300 and 370 K for each enantiomer. The (ψ_1, ψ_2) conformations recorded every 1 ps during the 100 ns simulations are shown in Fig. 3. (The first 10 ns of each simulation were taken to be equilibration time and were not included in our analysis.) We see that the data clusters around the conformers examined using QC calculations (red circles in Fig. 3a). At 300 K, not all of the conformers are accessible to the MD simulations, but at 370 K all nine conformers are observed for (*R*)-MPD and only one is not seen for (*S*)-MPD. Furthermore, no extraneous conformers are found confirming that our choice of conformers for the QC calculations was reasonable. Finally, at each temperature the (*R*)- and (*S*)-MPD results show approximately the expected mirror symmetries. More specifically, for the null hypothesis that the underlying distributions of the (*R*) and (*S*) conformers are the same, a chi-square test (see Supplementary Materials and Methods) reveals that this hypothesis is accepted with *p*-values of greater than 0.90 (at 300K) or 0.80 (at 370 K).

The relative free energy of each conformer was calculated by dividing the (ψ_1, ψ_2) conformational space into nine equal-sized bins (Fig. 3a). Since only one conformer lies in each bin, all observations in a given bin can be associated with a specific conformer. The molar Helmholtz free energy ΔF_i of conformer *i* relative to **1a** is given by (Frenkel & Smit, 1996)

$$\Delta F_i = -RT \ln \frac{N_i}{N_{1a}} \quad (1)$$

Here, N_i is the number of observation of conformer i and N_{1a} is the number of observations of conformer **1a**. R is the universal gas constant and T is the absolute temperature.

As we found with our QC calculations, the MD simulations reveal that **1a** is the most stable conformer and that there is a gap to the next most stable one (Table 3). When the temperature is changed from 300 K to 370 K this gap decreases, illustrating the increased importance of entropic contributions. Indeed, at 370 K the order of relative stability of the conformers is not the same as at 300 K.

Though the energy (QC) and free energy (MD) landscapes share global features, they differ in several ways. For example, the next most stable conformer in terms of energy is **3a**, while in terms of free energy it is **2a**. (We note that **2a** is the third most stable conformer energetically, only 1.4 kJ mol⁻¹ higher than **3a** *in vacuo* [Table 2]). Also, according to the MD results, **1c**, **2c** and **3c** are the least stable states and have similar free energies at 370 K, but the QC calculations show that **3c** is energetically more stable than the other two by about 10 kJ mol⁻¹, which is approximately the energy of a hydrogen bond. In fact, the distance between O2 and O4 atoms in **3c** is 2.7Å, suitable for the formation of a strong hydrogen bond. It is likely that the inclusion of entropic effects in the MD simulation renders **3c** less stable than would be predicted on purely energetic considerations.

To further compare the QC and MD results, we ran 100 MD annealing simulations on (*R*)-MPD in which the system was equilibrated at 370 K—where all nine conformers are observed—and slowly cooled to 0.1 K—where entropic contributions are small and energetic considerations determine the stability of the molecule. In 77 of these runs we found that the final conformation (green square in central bin of Fig. 3*a*) coincided with the **1a** conformation of the QC calculations (red circle in central bin of Fig. 3*a*), which is consistent with our previous result that **1a** is a global energy minimum.

In 20 of the remaining 23 runs, (*R*)-MPD reached a local minimum in the **2a** bin (the next most stable state in the MD simulations after **1a** [Table 3]), while in 3 runs it reached a **3b** conformation (the third most stable state). Based on the QC results we would have expected the order of states in the low temperature limit to be **1a** < **3a** < **2a** (in terms of increasing energy; Table 2). The difference may reflect the limitations of a classical force field in capturing the quantum mechanical aspects of atomic interactions.

Our computational results strongly suggest that **1a** should be the conformer most frequently observed in nature. To verify this hypothesis we examined the (ψ_1, ψ_2) conformations of (*R*)- and (*S*)-MPD found in the RCSB Protein Data Bank [PDB; (Berman *et al.*, 2000)]. As expected, we observed that majority of the conformers cluster around **1a** (Fig. 4), in agreement with a similar analysis made about a decade ago on the MPD molecules available at the time (Anand *et al.*, 2002). To further examine the MPD-protein interactions, we binned the PDB data as we did for the MD results and calculated the

relative Gibbs free energies of the conformers (Table 4). The results follow the pattern of the QC calculations and MD simulations in the absence of protein: conformer **1a** is the most stable and there is a gap (3.7 kJ mol^{-1} at 300K) between **1a** and the next most stable conformer. For the PDB results this next most stable conformer is **2a**, which in the same result we found in the MD simulations (Table 3).

In addition to providing information about the relative stability of the MPD conformers when strongly associated with protein, the PDB results allow us to examine possible chiral effects on this relative stability. In particular, we can ask whether there is a statistically significant difference in the distribution of conformers for co-crystallized (*R*)- and (*S*)-MPD. Since the MPD molecules in the PDB database are found in a chiral environment, a difference in the conformer distributions is possible. A chi-square test (Press *et al.*, 1992) on the binned data of the (*R*)- and (*S*)-MPD distributions (i.e., the number of times each of the nine conformers is observed) suggests that the null hypothesis—the underlying distributions of the (*R*) and (*S*) conformers are the same—should be accepted ($p = 0.11$). This result supports the hypothesis that any chiral interaction between MPD and proteins does not affect the relative stability of the conformers.

As a further check on the conformations of MPD, we also examined the Cambridge Structural Database [CSD; (Allen, 2002)]. While the small sample size precluded a detailed statistical analysis, we note that 8 of the 10 MPD molecules extracted from the CSD adopt conformer **1a**.

The QC, MD and database results all indicate that **1a** is the most stable conformer of MPD in both chiral and achiral environments. The other eight conformers are significantly less stable; the database analysis reveals that the probability of finding the MPD molecule in a conformation other than **1a** is less than 50% and the simulation results give much lower probabilities. We therefore decided to use **1a** exclusively to fit our electron density data for MPD co-crystallized with protein. As we show in Sec. 3.3, the choice leads to a reasonable fit of the experimental data.

Given the high resolution of our x-ray structures, we could have added one or even two more conformers with low occupancy to slightly improve the fit for the MPD molecules. However, we chose a conservative approach to the interpretation of the electron density map in order to achieve physically meaningful results and minimize the chance of encountering the many problems that can arise when analyzing protein-ligand complexes (Kleywegt, 2009). Our work highlights the need for a thorough conformational analysis of the ligand molecules complexed with macromolecular structures, and we support the recent appeal for reliable standard restraint libraries for ligand molecules found in the PDB (Jaskolski, 2013).

3.3. Lysozyme crystals and MPD interactions

When lysozyme is crystallized in Tris at pH 8.0, it forms tetragonal crystals with space group $P4_32_12$ and almost identical unit-cell parameters whether or not MPD is used and independent of the MPD stereochemistry (Table 5). This result is consistent with the findings of other investigators who have observed this crystalline arrangement for a broad set of solution conditions (Bujacz *et al.*, 2010; Helliwell & Tanley, 2013; Judge *et al.*, 1999; Michaux *et al.*, 2008; Tanley *et al.*, 2012; Weiss *et al.*, 2000). The structures of lysozyme obtained from the four conditions we have studied (namely, (*R*)-, (*S*)-, (*RS*)-MPD, and no MPD) are similar as well; the root-mean-square deviation between equivalent C_α atoms is less than 0.4 Å for any two of the structures (Supplementary Table S6).

There are, however, important differences between the crystals. Most importantly, the resolution and disorder (as measured by the mosaicity and B factor) vary with the precipitant used (Table 2). The highest quality crystals are produced when (*R*)-MPD is the precipitant. Furthermore, the pure enantiomers of MPD have different interactions with the protein. Both (*R*)-MPD and (*S*)-MPD form a crystal contact near F34, but a second molecule of (*R*)-MPD is found near W63 very close to the active site of the protein (Ogata *et al.*, 2013). No (*S*)-MPD is seen at this location, but a second molecule of (*S*)-MPD is found near W123 (Fig. 5). With (*RS*)-MPD as the precipitant, only (*R*)-MPD molecules are observed and they are found near F34 and W63, the same pattern as observed for pure (*R*)-MPD. We examine below each of the sites in detail where MPD is found.

3.3.1. F34 interaction site

This is a crystal contact site where MPD forms hydrogen bonds involving residues on two symmetry-related proteins: F34 and G22' (Fig. 6; for completeness the direct hydrogen bond between R114 and G22' is also shown). This site has been discussed previously by other investigators working at lower resolution with (*RS*)-MPD, but the results are contradictory: Weiss *et al.* find only (*R*)-MPD in the crystal (Weiss *et al.*, 2000), while Michaux *et al.* find only (*S*)-MPD (Michaux *et al.*, 2008).

Our high-resolution structures with pure (*R*)- and (*S*)-MPD allow us to clarify these conflicting results. We observe that the electron density is better defined for (*R*)-MPD (Fig. 6*a*) than is it for (*S*)-MPD (Fig. 6*b* and Supplementary Fig. S12), which is reflected in the higher occupancy of (*R*)-MPD (0.9 vs. 0.5). Indeed, we find that a water molecule (occupancy 0.5) at the C1 position of (*S*)-MPD is competing with (*S*)-MPD (for clarity, this water molecule is omitted from Fig. 6*b*). These results suggest that there is a preferential interaction between lysozyme and (*R*)-MPD at the F34 site and this suggestion is confirmed by our results with (*RS*)-MPD—we observe (*R*)-MPD at the site (Fig. 6*c*). The occupancy (0.55) is not as high as that of pure (*R*)-MPD, which may be due to several factors, such as the lower concentration of (*R*)-MPD in solution (half of that in pure (*R*)-MPD) and the competition with (*S*)-MPD for the site.

Also, just as we observed with pure (*S*)-MPD, it is possible that water is competing for the same site. When we crystallize lysozyme without any MPD, we observe a water molecule making equivalent hydrogen bonds (Fig. 6*d*). Nevertheless, MPD is a more effective crystallizing agent than water. Lysozyme crystals (200 μm) grew in about 5 days with MPD; crystals of approximately the same size took about two weeks to grow without MPD. In our previous work, we noticed a similar effect with thaumatin and the L and D enantiomers of sodium tartrate, where the same crystal habits form with and without the additives, but those grown with the additives are favored kinetically (Asherie *et al.*, 2009).

Given these results, we agree with the Weiss assignment (Weiss *et al.*, 2000) of (*R*)-MPD at the F34 site when (*RS*)-MPD is used as the additive (Fig. 6*e*). While it is possible that there is small fraction of (*S*)-MPD contributing to the electron density, assigning only (*S*)-MPD to the site, as Michaux *et al.* (Michaux *et al.*, 2008) have done, provides a poor fit to the electron density data. The problematic nature of their assignment can be seen by examining the B-factors of the atoms in the (*S*)-MPD, which are non-uniform and unusually high (Supplementary Fig. S13). When we produced an omit map using their data, we find that assigning (*R*)-MPD to the site provides a better fit to the electron density.

Another difference between the interactions of each enantiomer with the protein is evident from the different orientations of the two additives at the binding site (Fig. 6*a* and 6*b*), which lead to different intermolecular hydrogen bonding between MPD and the protein residues. The donor-acceptor pairs connecting the (*R*)-MPD and the protein are O2 and the carbonyl oxygen of F34, and O4 and the carbonyl oxygen of G22', whereas for (*S*)-MPD, the pairs are O4-F34 and O2-G22'.

As it is possible for O2 and O4 to make hydrogen bonds with either F34 or G22', we wondered why there is no evidence in the electron density for a rigid body rotation in which O2 and O4 exchange locations. We believe that such a rotation is unfavorable due to steric hindrance. For example, rotating (*R*)-MPD so that it makes the O4-F34 and O2-G22' hydrogen bonds observed with (*S*)-MPD would lead to a strong repulsion between the methyl group CM and the carbonyl O of K33.

3.3.2. W63 interaction site

Here MPD forms hydrogen bonds with W63 and N59 of the same protein. Even though it is not a crystal contact site, it may contribute to the differences observed between the various crystals because we find (*R*)-MPD at the site (occupancy 0.60) when it is the additive (Fig. 7*a*), but no (*S*)-MPD when it is the sole additive (Fig. 7*b*). Instead, we find two water molecules making equivalent hydrogen bonds to those found with (*R*)-MPD. Our (*RS*)-MPD results are consistent with this finding—we observe (*R*)-MPD at the site (Fig. 7*c*) with occupancy of 0.50.

Weiss *et al.* (Weiss *et al.*, 2000) find poorly defined electron density in this region that they assign to water molecules. Michaux *et al.* (Michaux *et al.*, 2008) observe more clearly defined density that they fit with (*S*)-MPD (Fig. 7*d*), but for this assignment C4 protrudes from the electron density (black arrow in Fig. 7*d*). As with the F34 site, we believe that (*R*)-MPD is a more appropriate assignment.

It is an open question as to why only (*R*)-MPD is observed at this site. We do not find any obvious factors that would exclude the other enantiomer as the region near W63 does not appear to be a traditional enantioselective binding site for MPD, a pocket in which only one enantiomer fits (Ali *et al.*, 2006; Haginaka, 2008). It is likely that more subtle effects are involved in the formation of a preferred diastereomeric complex between the additive and the protein (Lämmerhofer, 2010).

3.3.3. W123 interaction site

The only crystals where we can confidently assign MPD at this site are for those grown with (*S*)-MPD where the occupancy is 0.50 (Fig. 8 and Supplementary Fig. S14). For (*R*)-MPD, there is no significant density, while for (*RS*)-MPD the density is too poorly defined to make a definite assignment—we choose to assign water molecules. Weiss *et al.* (Weiss *et al.*, 2000) and Michaux *et al.* (Michaux *et al.*, 2008) also find poorly defined density at this site; the former group assigns a Tris molecule while the latter assigns a water molecule.

It is not clear what role this site plays in the crystal structure. There are no direct hydrogen bonds between MPD and the protein and only one indirect hydrogen bond to A122 through a water molecule. Furthermore, as with the W63 site, the mechanism of the enantioselective interaction between the protein and MPD remains to be elucidated.

3.3.4. Crystal quality

The enantioselective interactions of lysozyme with MPD affect the crystal quality. We find the highest resolution and least disordered crystals (as measured by the average protein B-factor and the mosaicity) are obtained with (*R*)-MPD (Table 6). This is true whether we use the maximum resolution limit data (Table 6) or compare the crystals at constant $I/\sigma I$ (Supplementary Table S7). The higher quality of the crystals obtained with (*R*)-MPD is consistent with the better crystal contact this enantiomer forms with the protein at the F34 site.

The other crystals are lower in quality. Those grown with (*S*)-MPD appear to be the worse ones overall, suggesting that (*S*)-MPD has a deleterious effect on crystal growth relative to not using any MPD. Data from a second set of crystals (Supplementary Table S7) supports this suggestion.

The crystals grown with (*RS*)-MPD by Weiss *et al.* (Weiss *et al.*, 2000) and Michaux *et al.* (Michaux *et al.*, 2008) have lower resolution and higher B-factors than our (*RS*)-MPD crystals, which is

probably due in part to the less pure lysozyme they use. (These authors do not report the mosaicity in their work, but in any case it would be difficult to compare mosaicities across beamlines as the x-ray beams have different divergences.) It is likely, however, that the use of a racemic additive as opposed to one that is enantiomerically pure adversely affects the crystal quality as well. When crystallizing thaumatin with the stereoisomers of sodium tartrate, we found that the highest quality crystals formed with enantiomerically pure precipitants (Asherie *et al.*, 2009).

3.4. Chirality and protein crystallization: comments and recommendations

The use of chirality to influence the crystallization of small molecules is an active field of study with a distinguished history (Perez-Garcia & Amabilino, 2002). Indeed, Louis Pasteur discovered the molecular basis of chirality in 1848 through a crystallization experiment (Gal, 2008, 2011). In contrast, much less work has been done on the role of chirality in protein crystallization. Apart from our own research, the only other systematic approach we are aware of that uses chirality to control protein crystallization is the racemic crystallization of synthetic proteins (Pentelute *et al.*, 2008; Sawaya *et al.*, 2012; Yeates & Kent, 2012). If the protein of interest is small enough and has a sufficient number of disulfide bonds to ensure proper folding, it can be produced by total chemical synthesis. Since the protein is assembled artificially, it can be made as two enantiomers—one consisting of naturally occurring L-amino acids and the other with D-amino acids—and then crystallized as enantiomeric pairs. This approach has made it easier to crystallize and solve the structure of more than a dozen proteins (Yeates & Kent, 2012).

Further indications that chirality is a useful tool in protein crystallization can be gleaned from the literature. For example, to produce high-resolution crystals of the membrane protein complex Photosystem I in β -dodecylmaltoside, the lipid must be of sufficient stereochemical purity—the α stereoisomer content must be below 10% (Fromme & Witt, 1998). One difficulty that arises during a literature search is that the stereochemical identity of the additives used is often omitted by the manufacturer (especially in the case of crystallization kits) or by the investigator. We note that chiral molecules are commonly found in commercially available kits. In the 180 kits we examined from eight manufacturers—Hampton Research, Qiagen, Jena Biosciences, Molecular Dimensions, Sigma-Aldrich, Microlytic, Anatrace and Rigaku—we found at least one chiral molecule in 134 kits (74% of all kits). Given the widespread inclusion of chiral molecules in kits and the possible usefulness of chirality in a protein crystallization experiment, we encourage other investigators to specify the absolute stereochemical configuration of all chemicals used when reporting their experimental results.

In addition to a general lack of information about chirality, we also encountered nomenclature problems related to how the molecule 2-methyl-2,4-pentanediol is described in the PDB. Inconsistent numbering schemes are often used, e.g., in PDB ID 1JLT, where the two MPD molecules in the

structure are numbered differently. In particular, CM and C1 are regularly switched, making it harder to analyze the conformations of the additives and obscuring the structural information that one molecule is the mirror image of the other. The numbering we chose (Fig. 1) follows the IUPAC recommendation for branched hydrocarbons (IUPAC, 1979) and appropriately highlights the **1a** conformation. In fact, we had to repeatedly request the PDB to use this numbering for (*R*)-MPD in our structures as when we initially deposited them the numbering was switched. The tendency of the PDB to perpetuate incorrect or confusing numbering schemes has been recently noted (Jaskolski, 2013) and should be corrected.

Another problem with nomenclature and chiral molecules in the PDB arises with the three letter ligand IDs used to identify the molecules. At the time of writing, a search of the PDB for “MPD,” which is the ligand ID for (*S*)-MPD, finds 826 structures; a search for “MRD,” the ligand ID for (*R*)-MPD, finds only 309 structures. This difference may be due to a real chiral effect, but since most of the structures are not high resolution, it is unlikely that this effect can always be seen. That is, the density for the ligand could be fit with either enantiomer. (For all experiments apart from ours, (*RS*)-MPD is the additive used, so in principle either enantiomer could be present in the x-ray structure.) Indeed, for the high resolution data we analyze, we find almost equal numbers of (*R*)- and (*S*)-MPD interacting with proteins. The preponderance of (*S*)-MPD in the PDB probably reflects a linguistic bias: when people fit their data, they use MPD—i.e., (*S*)-MPD—because it is the acronym by which most people refer to the molecule 2-methyl-2,4-pentandiol. To avoid such problems, we suggest that the PDB should name enantiomers, and more generally stereoisomers, using abbreviations that don't introduce bias. This is particularly important given the large number of chiral molecules in the PDB.

There are 90 chiral molecules in the top 200 PDB ligands (ranked by ligand hits, i.e., the number of times the ligand is reported in a PDB structure) and approximately 20% of ligand hits involve chiral molecules. We believe that since chiral molecules are common, possible chiral effects in protein crystallization should be explored in detail. Furthermore, it seems reasonable to explore more general stereochemical effects beyond enantiomerism. Given the prevalence of sugars as ligands in the PDB, we consider the stereoisomerism of sugars as an interesting possibility to consider when crystallizing proteins.

While the PDB protein structures and ligand list offer a useful starting point for choosing candidate chiral ligands, they provide only a partial view of the role of chiral molecules in protein crystallization. It is possible for chiral effects to be present in solution during protein nucleation, but that the final crystal does not incorporate the chiral additive. Indeed, we have observed this with thaumatin and tartrate. The addition of L-tartrate to thaumatin produces bipyramidal crystals that incorporate the additive in the lattice. The crystals have normal solubility and a tetragonal space group. Addition of D-tartrate leads instead to the formation of prismatic crystals with retrograde

solubility and an orthorhombic space group; these crystals do not contain any tartrate. (Asherie, Ginsberg, Blass, *et al.*, 2008; Asherie, Ginsberg, Greenbaum, *et al.*, 2008; Asherie *et al.*, 2009).

We focus here on high-resolution structures (resolution better than 1.5 Å) because they allow us to determine the stereochemistry and conformation of MPD with minimal uncertainty and therefore we are able to analyze chiral effects in detail. By doing so, we do not mean to imply that chiral effects are confined only to high-resolution structures. On the contrary, chiral effects span the range from the obvious (some of which can be seen with the naked eye) to the subtle. This is well known in small molecule systems and by studying different protein-additive pairs we expect to find that it holds for protein systems as well.

Further work is needed to fully understand the mechanism by which chirality affects protein crystallization. Chiral effects are often clear at crystal contacts, but these only account for only a small part of protein-additive interactions—we estimate the fraction of protein structures with at least one crystal contact by a chiral molecule to be about 5% (Carugo & Djinovic-Carugo, 2014). A more common situation is one in which two enantiomers interact with the protein at different sites, but these are not crystal contact sites; this is the case for the W63 and W123 interaction sites discussed in this work. And as we mentioned above, chiral molecules can also have an effect in the solution phase.

We appreciate that working with enantiomerically pure additives is expensive. Cost is one possible reason why crystallization experiments with MPD have been thus far carried out only with the racemate. At the time of writing, the cost per gram of 99% pure (*R*)-MPD from Sigma-Aldrich (cat. no. 252840) is more than 3000 times that of similar purity (*RS*)-MPD (cat. no. 112100). Nevertheless, given the potential benefits, some way to assess chiral effects should be incorporated into a crystallization experiment, and we expect that cost will diminish with increased demand for enantiomerically pure additives. If a full screening of crystallization conditions with the separate enantiomers of the additive under study is prohibitively expensive, we suggest that the initial screen be carried out with the cheaper racemate; promising conditions may then be optimized with the pure enantiomers. We are happy to provide small amounts of pure (*R*)- and (*S*)-MPD to members of the community.

4. Conclusion

We crystallized lysozyme with (*R*)-, (*S*)- and (*RS*)-MPD. We also grew crystals without MPD under similar conditions. All four crystalline arrangements obtained have the same space group and almost identical unit-cell parameters. The crystals grown with (*R*)-MPD have the highest resolution and least disorder suggesting a preferential interaction between lysozyme and this enantiomer of MPD. This idea is confirmed by the x-ray structures, which show that the two enantiomers interact differently

with the protein. Our findings support the hypothesis that chiral interactions with chiral additives are important in protein crystallization.

Acknowledgements We thank Charles Ginsberg and Samuel Blass for help in the initial stages of this project, and Shekhar Garde and Amish Patel for guidance on setting up molecular dynamics simulations. We also thank Jianfeng Jiang and Mark Harris for helpful discussions. N.A. gratefully acknowledges financial support from the National Science Foundation (DMR 1206416) and Yeshiva University. Computational resources were provided by the Dr. Bernard W. Gamson Computational Science Center at Yeshiva University. We thank the staff of the National Synchrotron Light Source, Brookhaven National Laboratory for their continuous support. The NSLS is supported by the U.S. Department of Energy, Office of Basic Energy Sciences, under contract no. DE-AC02-98CH10886. The NIGMS East Coast Structural Biology Facility, the X6A beamline, is funded under contract no. GM-0080.

Accession Codes

Lysozyme without MPD, 4B49; lysozyme with (*R*)-MPD, 4B4E; lysozyme with (*S*)-MPD, 4B4I; lysozyme with (*RS*)-MPD, 4B4J.

Table 1 Characterization of (*R*)-, (*S*)- and (*RS*)-MPD

	Chemical Purity	Enantiomeric Ratio	$[\alpha]_D^{20}$ (c 1.0, H ₂ O)
(<i>R</i>)-MPD	99.5%	99.9:0.1	-18.8 ± 0.2
(<i>S</i>)-MPD	99.7%	99.9:0.1	19.0 ± 0.2
(<i>RS</i>)-MPD	99.9%	50:50*	0.0 ± 0.2

*theoretical value (not measured)

Table 2 Relative energies of the conformers of (*R*)-MPD from QC calculations.

Conformer	ΔE (kJ mol ⁻¹)	ΔE (kJ mol ⁻¹)
	<i>in vacuo</i>	in water (PCM*)
1a	0.00	0.00
3a	12.41	14.93
2a	13.86	15.17
3c	14.46	15.91
3b	17.40	17.46
1b	19.53	19.40
2b	23.19	20.74
1c	23.45	24.48
2c	27.77	27.40

*PCM: polarizable continuum model

Table 3 Relative Helmholtz free energies of the conformers of (*R*)-MPD from MD simulations.

Conformer	ΔF (kJ mol ⁻¹)	
	300 K	370 K
1a	0.00	0.00
2a	5.93	3.41
3b	7.55	5.89
3a	7.92	6.46
2b	7.99	5.73
1b	8.75	8.16
1c	20.07	18.88
2c	—*	17.54
3c	—*	18.45

* conformer not observed

Table 4 Relative Gibbs free energies of the conformers of (*R*)- and (*S*)-MPD extracted from the PDB.

Conformer	ΔG (kJ mol ⁻¹)
	300K
1a	0.00
2a	3.70
3a	4.71
3c	6.99
1b	7.33
1c	7.33
2c	7.33
2b	7.71
3b	8.72

Table 5 Crystallographic data and refinement statistics

PDB entry	4B49	4B4E	4B4I	4B4J
MPD added	none	(<i>R</i>)	(<i>S</i>)	(<i>RS</i>)
<i>Data Collection</i>				
Space group	<i>P</i> 4 ₃ 2 ₁ 2			
Unit cell dimensions (Å) <i>a</i> = <i>b</i> , <i>c</i> (Å); ($\alpha = \beta = \gamma = 90^\circ$)	76.84 38.69	77.53 37.89	77.44 37.94	77.67 37.70
Resolution (Å) ^a	20.00-1.15 (1.17-1.15)	15.00-1.00 (1.02-1.00)	30.00-1.20 (1.22-1.20)	30.00-1.25 (1.27-1.25)
Total reflections	562743	853125	512028	456741
Unique reflections ^a	41718 (2040)	62397 (3076)	36597 (1806)	32449 (1584)
R _{merge} (%) ^a	0.08 (0.76)	0.07 (0.82)	0.08 (0.79)	0.06 (0.56)
I/ σ I ^a	41.5 (3.2)	43.3 (2.5)	45.1 (3.6)	45.9 (5.5)
Completeness (%) ^a	99.8 (99.1)	99.3 (99.0)	99.7 (100.0)	99.8 (99.6)
Redundancy ^a	13.5 (10.9)	13.7 (11.2)	14.0 (12.7)	14.1 (13.2)
Mosaicity (°)	0.32	0.26	0.46	0.43
B factor (Å ²) (Overall)	15.5	13.4	17.2	15.1
V _M (Å ³ /Da) / Solvent content (%)	2.03 / 39.6	2.03 / 39.6	2.03 / 39.4	2.03 / 39.3
<i>Refinement</i>				
Resolution (Å) ^a	18.67-1.15 (1.18-1.15)	13.30-1.00 (1.03-1.00)	21.49-1.20 (1.23-1.20)	27.05-1.25 (1.28-1.25)
Reflections [R _{cryst} + R _{free} (5%)]	39425 + 2089	59136 + 3155	34682 + 1825	30732 + 1643
R _{cryst} / R _{free} ^a	12.7 / 15.1 (22.2 / 25.6)	12.4 / 14.4 (25.0 / 25.7)	12.9 / 16.7 (18.8 / 22.1)	13.05 / 15.57 (18.1 / 22.7)
Number of atoms				
Protein (no. of residues) ^b	1001 (129)	1000 (129)	1000 (129)	1001 (129)
MPD ^c	—	16 (2; <i>R</i>)	16 (2; <i>S</i>)	16 (2; <i>R</i>)
Ions / Ligands (no. of molecules)	11 (4)	3 (3)	2 (2)	2 (2)
Water	267	196	188	162
B factors (Å ²)				
Protein	12.9	11.9	15.2	13.7
MPD	—	12.3	21.4	13.1
Ions / Ligands	13.1	14.2	17.7	15.4
Water	26.2	21.6	28.3	24.6
RMS deviation from ideal				
Bond length (Å)	0.009	0.008	0.007	0.007
Bond angles (°)	1.349	1.306	1.214	1.272
Ramachandran plot				
Most favored (%)	90.3	90.3	88.5	87.6
Additionally favored (%)	9.7	9.7	11.5	12.4
Disallowed (%)	0.0	0.0	0.0	0.0

^aNumber in parentheses refers to the highest resolution shell.

^bAtom OXT (residue L129) was omitted during the refinement for structures 4B4E and 4B4J.

^cIn parentheses: (no. of molecules in the structure; enantiomer).

Table 6 Comparison of crystal quality

Investigators	MPD additive	Maximum resolution (Å)	Overall B factor (Å ²)	Mosaicity (°)
This work	(<i>R</i>)-MPD	1.00	13.4	0.26
This work	none	1.15	15.5	0.32
This work	(<i>S</i>)-MPD	1.20	17.2	0.46
This work	(<i>RS</i>)-MPD	1.25	15.1	0.43
Weiss <i>et al.</i> ^a	(<i>RS</i>)-MPD	1.64	19.0	—
Michaux <i>et al.</i> ^b	(<i>RS</i>)-MPD	1.75	20.2	—

^aPDB ID 1DPW (Weiss *et al.*, 2000).

^bPDB ID 3B72 (Michaux *et al.*, 2008).

Figure 1 Schematic representation of (*R*)- and (*S*)-MPD. The carbon atoms are numbered according to the convention used in this work and the torsion angles (ψ_1, ψ_2) are represented by red arrows. CM is the unlabelled methyl carbon attached to C2 by a dashed line; the oxygen atoms attached to C2 and C4 are O2 and O4, respectively; and the chiral center is at C4.

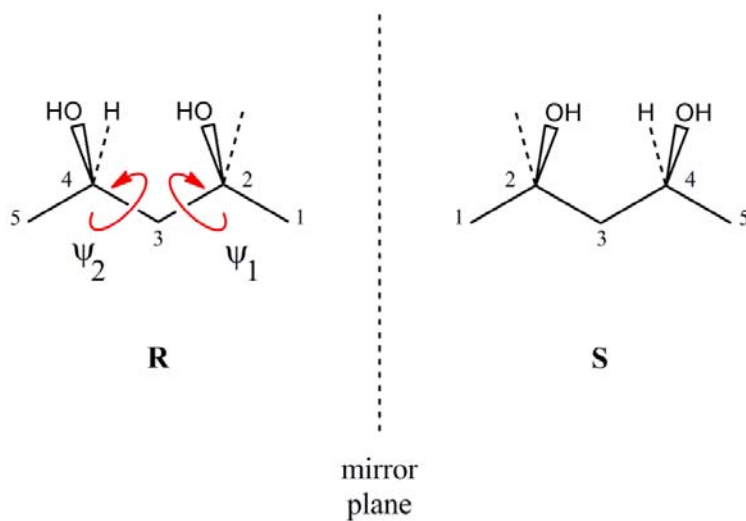


Figure 2 The conformers of MPD studied by quantum chemical calculations. Each conformer is denoted by a two symbol code (number and letter) that represents approximately the torsion angles (ψ_1, ψ_2) of the initial conformation used in the calculation. The numbers 1, 2 and 3 correspond to $\psi_1 = 180^\circ, 300^\circ$ and 60° , respectively; the letters a, b and c correspond to $\psi_2 = 180^\circ, 60^\circ$ and 300° , respectively. (For example, **1a** is the $(180^\circ, 180^\circ)$ conformer shown in Fig. 1.) To interconvert two adjacent structures, a rotation is performed about the carbon-carbon bond given in square brackets. For clarity, only C2, C3 and C4 are numbered; C1 is shown in red, while CM and C5 (which is adjacent to C4) are shown in black.

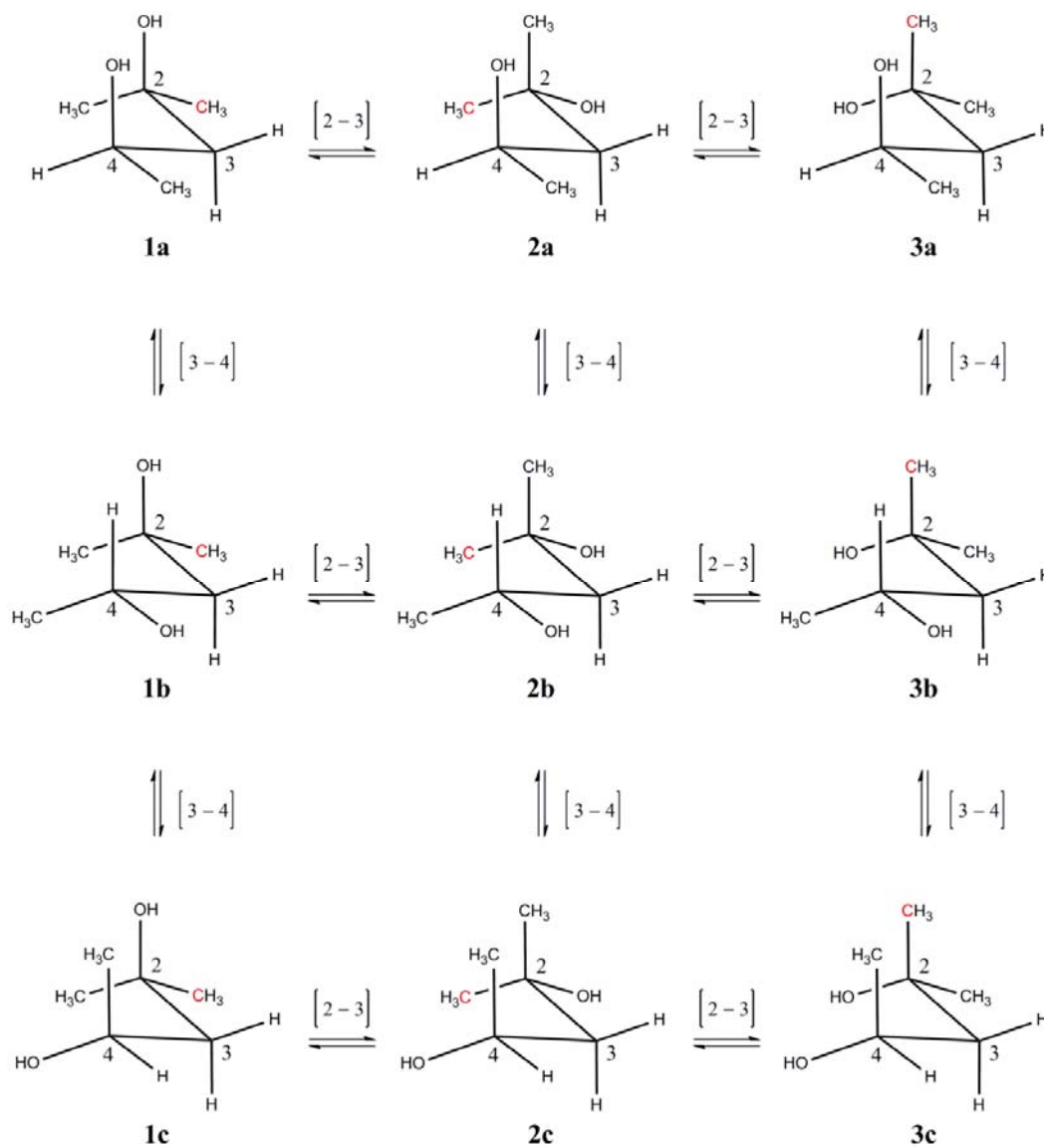


Figure 3 The conformations of MPD from MD simulations *in vacuo*. (a) (R)-MPD at 300 K; (b) (R)-MPD at 370 K; (c) (S)-MPD at 300 K; (d) (S)-MPD at 370 K. In panel (a), the dashed lines mark the nine bins used in the free energy calculations. The red circles are the nine locally stable conformers obtained from quantum chemical calculations; the corresponding label for each conformer is shown in bold. The results of the simulated annealing experiments lie within the green squares.

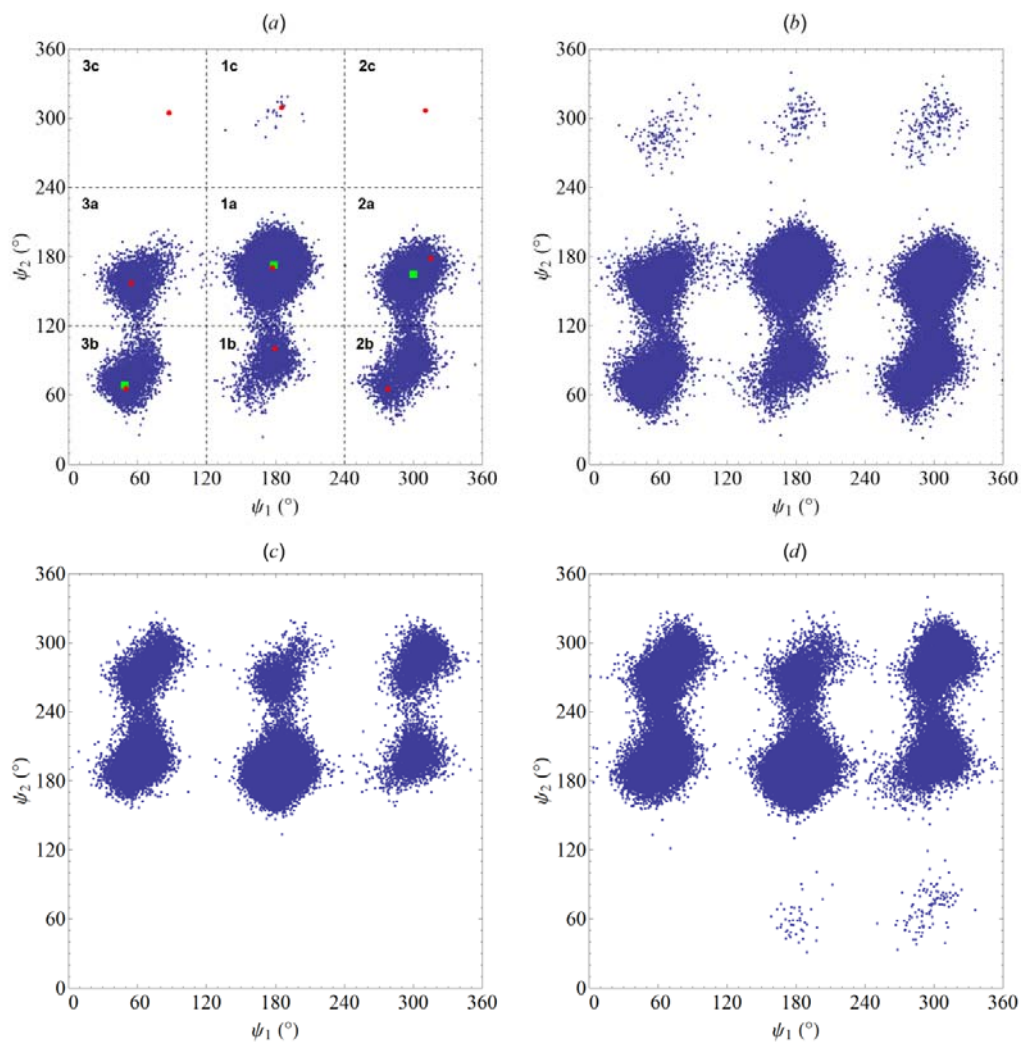


Figure 4 The conformations of MPD from the Protein Data Bank. The two enantiomers are shown in different colors: (*R*)-MPD (red) and (*S*)-MPD (blue). The dashed lines mark the nine bins used in the free energy calculations (cf. Figure 3a).

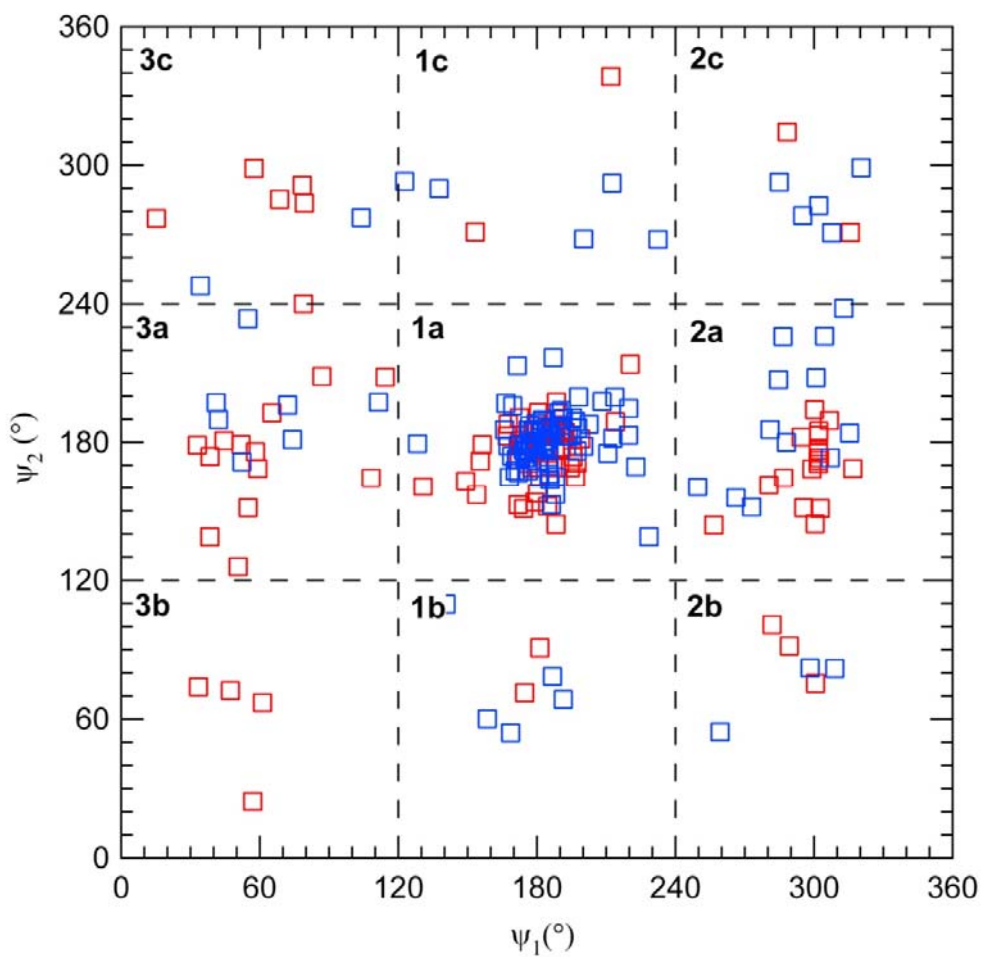


Figure 5 Overall structures of lysozyme with the enantiomers of MPD. A ribbon diagram of the C_α backbone is shown for crystals grown with (*R*)-MPD (blue) and (*S*)-MPD (green). The MPD molecules associated with each structure are shown in the same color as the protein backbone.

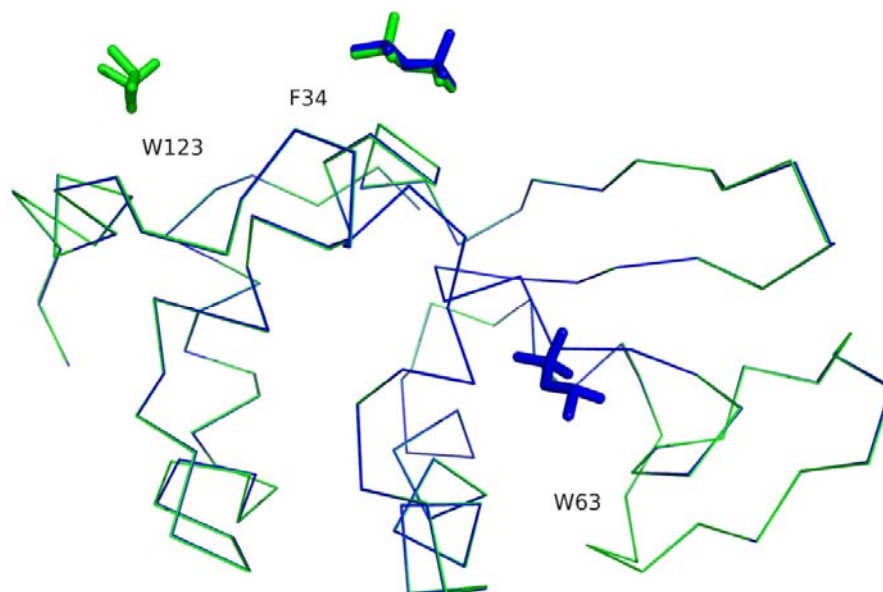


Figure 6 The crystal contact site near F34. Two symmetry related proteins (shown with green and purple carbon atoms) interact through hydrogen bonds (dashed orange lines). Panels (a–d) depict the results from the current work with different additives. (a) (*R*)-MPD; (b) (*S*)-MPD; (c) (*RS*)-MPD; (d) no MPD added. The red sphere in panel (d) is the O atom of a water molecule. For comparison the results of (e) Weiss *et al.* (Weiss *et al.*, 2000). and (f) Michaux *et al.* (Michaux *et al.*, 2008)—both of whom used (*RS*)-MPD—are also presented. The $2F_o - F_c$ density is shown as a gray mesh contoured at 1.5σ .

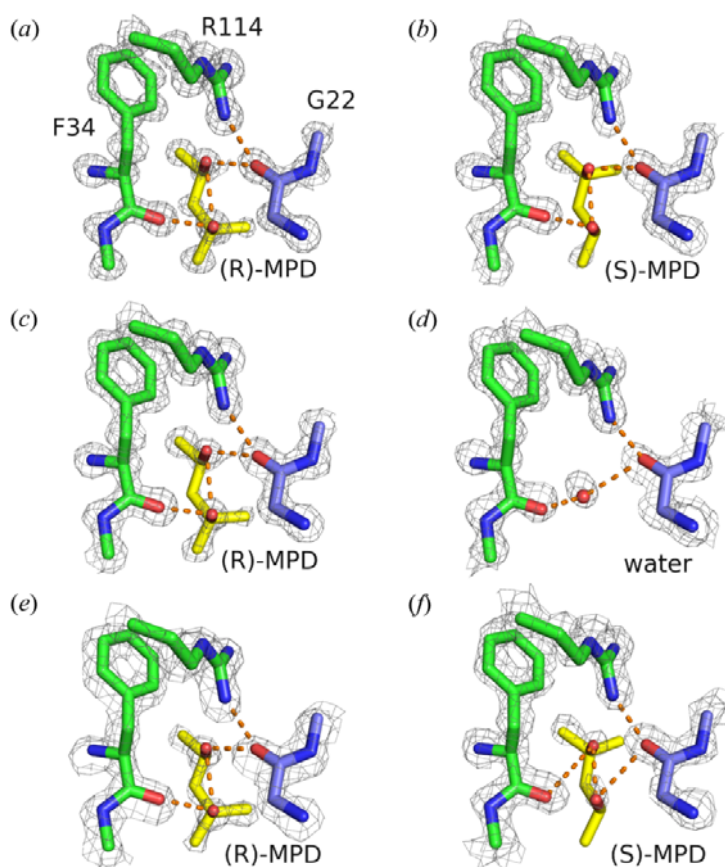


Figure 7 The interaction site near W63. Panels (a-c) depict the results from the current work with different additives. (a) (*R*)-MPD; (b) (*S*)-MPD; (c) (*RS*)-MPD. The red spheres in panel (b) are the O atoms of water molecules. For comparison the results of (d) Michaux *et al.* (Michaux *et al.*, 2008) — which used (*RS*)-MPD—is also presented. The $2F_o - F_c$ density is shown as a gray mesh contoured at 1.5σ except for the (*S*)-MPD molecule in (d), which is shown at 1.0σ . This is done to highlight that C4 (denoted by arrow) protrudes from the density.

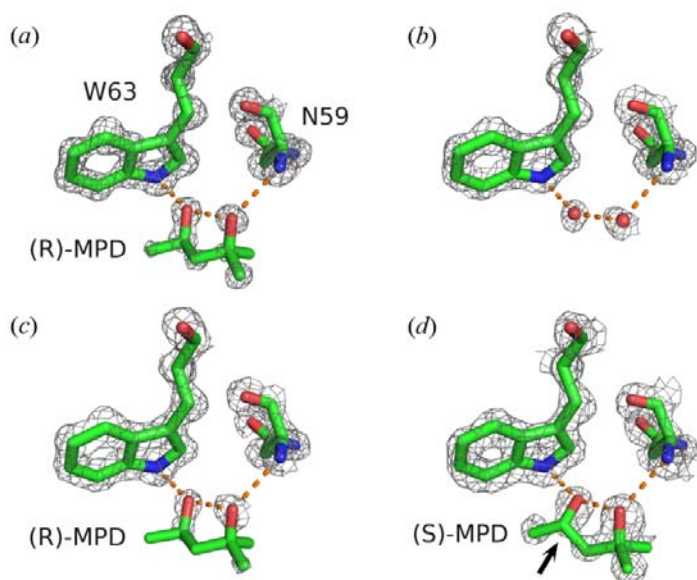
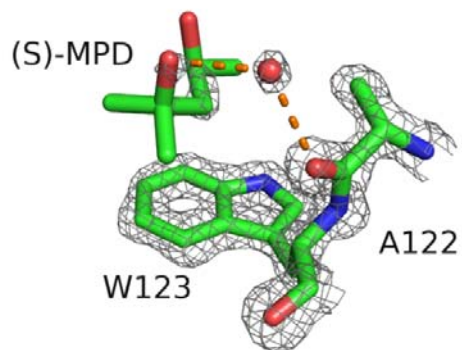


Figure 8 The interaction site near W123. (*S*)-MPD interacts with the protein through hydrogen bonds (dashed orange lines). The red sphere is the O atom of a water molecule. The $2F_o - F_c$ density is shown as a gray mesh contoured at 1.5σ . For clarity the intramolecular hydrogen bond between O2 and O4 of (*S*)-MPD is not shown.



- Addadi, L., Berkovitch-Yellin, Z., Domb, N., Gati, E., Lahav, M. & Leiserowitz, L. (1982). *Nature (London, U. K.)* **296**, 21-26.
- Ali, I., Kumerer, K. & Aboul-Enein, H. Y. (2006). *Chromatographia* **63**, 295-307.
- Allen, F. H. (2002). *Acta Crystallogr B* **58**, 380-388.
- Amharar, Y., Grandeur, A., Sanselme, M., Petit, S. & Coquerel, G. (2012). *The Journal of Physical Chemistry B* **116**, 6027-6040.
- Anand, K., Pal, D. & Hilgenfeld, R. (2002). *Acta Crystallogr D* **58**, 1722-1728.
- Asherie, N., Ginsberg, C., Blass, S., Greenbaum, A. & Knafo, S. (2008). *Cryst. Growth Des.* **8**, 1815-1817.
- Asherie, N., Ginsberg, C., Greenbaum, A., Blass, S. & Knafo, S. (2008). *Cryst. Growth Des.* **8**, 4200-4207.
- Asherie, N., Jakoncic, J., Ginsberg, C., Greenbaum, A., Stojanoff, V., Hrnjez, B. J., Blass, S. & Berger, J. (2009). *Cryst. Growth Des.* **9**, 4189-4198.
- Aune, K. C. & Tanford, C. (1969). *Biochemistry* **8**, 4579-4585.
- Berman, H. M., Westbrook, J., Feng, Z., Gilliland, G., Bhat, T. N., Weissig, H., Shindyalov, I. N. & Bourne, P. E. (2000). *Nucleic Acids Res.* **28**, 235-242.
- Blackmond, D. G. (2011). *Philos T R Soc B* **366**, 2878-2884.
- Brittain, H. G. (2013). *Chirality* **25**, 8-15.
- Brooks, W. H., Guida, W. C. & Daniel, K. G. (2011). *Curr. Top. Med. Chem.* **11**, 760-770.
- Bruno, I. J., Cole, J. C., Edgington, P. R., Kessler, M., Macrae, C. F., McCabe, P., Pearson, J. & Taylor, R. (2002). *Acta Crystallogr B* **58**, 389-397.
- Bujacz, G., Wrzesniewska, B. & Bujacz, A. (2010). *Acta Crystallogr D* **66**, 789-796.
- Bussi, G., Zykova-Timan, T. & Parrinello, M. (2009). *J. Chem. Phys.* **130**.
- Candoni, N., Grossier, R., Hammadi, Z., Morin, R. & Veessler, S. (2012). *Protein Pept. Lett.* **19**, 714-724.
- Carugo, O. & Djinic-Carugo, K. (2014). *J. Appl. Crystallogr.* **47**, 458-461.
- Chan, M., Fazio, V. J. & Newman, J. (2013). *Cryst. Growth Des.* **13**, 1290-1294.
- Chayen, N. E. (2002). *Trends Biotechnol.* **20**, 98-98.
- Chayen, N. E. (2004). *Curr. Opin. Struct. Biol.* **14**, 577-583.
- Chayen, N. E. & Saridakis, E. (2001). *J. Cryst. Growth* **232**, 262-264.
- Chayen, N. E. & Saridakis, E. (2008). *Nat. Methods* **5**, 147-153.
- Chayen, N. E., Saridakis, E., El-Bahar, R. & Nemirovsky, Y. (2001). *J. Mol. Biol.* **312**, 591-595.
- Clark, T., Chandrasekhar, J., Spitznagel, G. W. & Schlever, P. v. R. (1983). *J. Comput. Chem.* **4**, 294-301.
- Dold, P., Ono, E., Tsukamoto, K. & Sasaki, G. (2006). *J. Cryst. Growth* **293**, 102-109.
- Dumetz, A. C., Chockla, A. M., Kaler, E. W. & Lenhoff, A. M. (2009). *Cryst. Growth Des.* **9**, 682-691.
- Eicke, M. J., Levilain, G. & Seidel-Morgenstern, A. (2013). *Cryst. Growth Des.* **13**, 1638-1648.
- Emsley, P., Lohkamp, B., Scott, W. G. & Cowtan, K. (2010). *Acta Crystallogr D* **66**, 486-501.
- Essmann, U., Perera, L., Berkowitz, M. L., Darden, T., Lee, H. & Pedersen, L. G. (1995). *J. Chem. Phys.* **103**, 8577-8593.
- Frenkel, D. & Smit, B. (1996). *Understanding Molecular Simulation: From Algorithms to Applications*. San Diego: Academic Press.
- Frisch, M. J., Trucks, G. W., Schlegel, H. B., Scuseria, G. E., Robb, M. A., Cheeseman, J. R., Scalmani, G., Barone, V., Mennucci, B., Petersson, G. A., Nakatsuji, H., Caricato, M., Li, X., Hratchian, H. P., Izmaylov, A. F., Bloino, J., Zheng, G., Sonnenberg, J. L., Hada, M., Ehara, M., Toyota, K., Fukuda, R., Hasegawa, J., Ishida, M., Nakajima, T., Honda, Y., Kitao, O., Nakai, H., Vreven, T., Montgomery Jr., J. A., Peralta, J. E., Ogliaro, F., Bearpark, M. J., Heyd, J., Brothers, E. N., Kudin, K. N., Staroverov, V. N., Kobayashi, R., Normand, J., Raghavachari, K., Rendell, A. P., Burant, J. C., Iyengar, S. S., Tomasi, J., Cossi, M., Rega, N., Millam, N. J., Klene, M., Knox, J. E., Cross, J. B., Bakken, V., Adamo, C., Jaramillo, J., Gomperts, R., Stratmann, R. E., Yazyev, O., Austin, A. J., Cammi, R., Pomelli, C., Ochterski, J. W., Martin, R. L., Morokuma, K., Zakrzewski, V. G., Voth, G. A., Salvador, P., Dannenberg, J. J., Dapprich, S., Daniels, A. D., Farkas, Ö., Foresman, J. B., Ortiz, J. V., Cioslowski, J. & Fox, D. J. (2009). *Gaussian 09*.
- Fromme, P. & Witt, H. T. (1998). *Bba-Bioenergetics* **1365**, 175-184.
- Gabanyi, M. J., Adams, P. D., Arnold, K., Bordoli, L., Carter, L. G., Flippen-Andersen, J., Gifford, L., Haas, J., Kouranov, A., McLaughlin, W. A., Micallef, D. I., Minor, W., Shah, R., Schwede, T., Tao, Y. P., Westbrook, J. D., Zimmerman, M. & Berman, H. M. (2011). *J. Struct. Funct. Genomics* **12**, 45-54.
- Gal, J. (2008). *Chirality* **20**, 5-19.
- Gal, J. (2011). *Chirality* **23**, 1-16.
- Ghatak, A. S. & Ghatak, A. (2011). *Ind. Eng. Chem. Res.* **50**, 12984-12989.
- Gou, L., Lorenz, H. & Seidel-Morgenstern, A. (2012). *Cryst. Growth Des.* **12**, 5197-5202.
- Haginaka, J. (2008). *Journal of Chromatography B* **875**, 12-19.
- Helliwell, J. R. & Tanley, S. W. M. (2013). *Acta Crystallogr D* **69**, 121-125.
- Hess, B., Kutzner, C., van der Spoel, D. & Lindahl, E. (2008). *J. Chem. Theory Comput.* **4**, 435-447.
- IUPAC (1979). *Nomenclature of Organic Chemistry*. Oxford: Pergamon Press.
- Jaskolski, M. (2013). *Acta Crystallographica Section D* **69**, 1865-1866.
- Jorgensen, W. L., Maxwell, D. S. & TiradoRives, J. (1996). *J. Am. Chem. Soc.* **118**, 11225-11236.
- Jorgensen, W. L. & Tiradorives, J. (1988). *J. Am. Chem. Soc.* **110**, 1657-1666.
- Judge, R. A., Forsythe, E. L. & Pusey, M. L. (1998). *Biotechnol. Bioeng.* **59**, 776-785.
- Judge, R. A., Jacobs, R. S., Frazier, T., Snell, E. H. & Pusey, M. L. (1999). *Biophys. J.* **77**, 1585-1593.
- Kleywegt, G. J. (2009). *Acta Crystallogr D* **65**, 134-139.
- Kleywegt, G. J., Harris, M. R., Zou, J. Y., Taylor, T. C., Wahlby, A. & Jones, T. A. (2004). *Acta Crystallogr D* **60**, 2240-2249.
- Lämmerhofer, M. (2010). *J Chromatogr A* **1217**, 814-856.
- Laskowski, R. A., Macarthur, M. W., Moss, D. S. & Thornton, J. M. (1993). *J. Appl. Crystallogr.* **26**, 283-291.
- Levilain, G., Eicke, M. J. & Seidel-Morgenstern, A. (2012). *Cryst. Growth Des.* **12**, 5396-5401.
- Liang, M., Jin, F. M., Liu, R., Yu, Y. J., Su, R. X., Wang, L. B., Qi, W. & He, Z. M. (2013). *Bioprocess Biosyst. Eng.* **36**, 91-99.
- Lorber, B., Skouri, M., Munch, J. P. & Giege, R. (1993). *J. Cryst. Growth* **128**, 1203-1211.
- Lorenz, H. & Seidel-Morgenstern, A. (2014). *Angew Chem Int Edit* **53**, 1218-1250.
- Magay, E. & Yoon, T. S. (2011). *J. Appl. Crystallogr.* **44**, 252-253.
- Mandado, M., Mosquera, R. A. & Van Alsenoy, C. (2006). *Tetrahedron* **62**, 4243-4252.
- McPherson, A. (1999). *Crystallization of Biological Macromolecules*. Cold Spring Harbor: Cold Spring Harbor Laboratory Press.

- McPherson, A., Nguyen, C., Cudney, R. & Larson, S. B. (2011). *Cryst. Growth Des.* **11**, 1469-1474.
- Michaux, C., Pouyez, J., Wouters, J. & Prive, G. G. (2008). *Bmc Struct Biol* **8**, 29-36.
- Mo, Y. R. (2010). *J. Org. Chem.* **75**, 2733-2736.
- Møller, C. & Plesset, M. S. (1934). *Physical Review* **46**, 618-622.
- Murshudov, G. N., Vagin, A. A. & Dodson, E. J. (1997). *Acta Crystallogr D* **53**, 240-255.
- Ogata, M., Umemoto, N., Ohnuma, T., Numata, T., Suzuki, A., Usui, T. & Fukamizo, T. (2013). *J. Biol. Chem.* **288**, 6072-6082.
- Otwinowski, Z. & Minor, W. (1997). *Methods Enzymol.* **276**, 307-326.
- Parmar, A. S., Gottschall, P. E. & Muschol, M. (2007). *Biophys. Chem.* **129**, 224-234.
- Pentelute, B. L., Gates, Z. P., Tereshko, V., Dashnau, J. L., Vanderkooi, J. M., Kossiakoff, A. A. & Kent, S. B. H. (2008). *J. Am. Chem. Soc.* **130**, 9695-9701.
- Perez-Garcia, L. & Amabilino, D. B. (2002). *Chem. Soc. Rev.* **31**, 342-356.
- Press, W. H., Teukolsky, S. A., Vetterling, W. T. & Flannery, B. P. (1992). *Numerical Recipes in C: The Art of Scientific Computing*, 2nd ed. Cambridge, UK: Cambridge University Press.
- Pusey, M. L., Liu, Z. J., Tempel, W., Praissman, J., Lin, D. W., Wang, B. C., Gavira, J. A. & Ng, J. D. (2005). *Prog. Biophys. Mol. Biol.* **88**, 359-386.
- Ryckaert, J. P., Ciccotti, G. & Berendsen, H. J. C. (1977). *J. Comput. Phys.* **23**, 327-341.
- Salam, A. & Deleuze, M. S. (2002). *J. Chem. Phys.* **116**, 1296-1302.
- Sauter, C., Otalora, F., Gavira, J. A., Vidal, O., Giege, R. & Garcia-Ruiz, J. M. (2001). *Acta Crystallogr D* **57**, 1119-1126.
- Sawaya, M. R., Pentelute, B. L., Kent, S. B. H. & Yeates, T. O. (2012). *Acta Crystallogr D* **68**, 62-68.
- Scalmani, G. & Frisch, M. J. (2010). *J. Chem. Phys.* **132**.
- Tanley, S. W. M., Schreurs, A. M. M., Kroon-Batenburg, L. M. J., Meredith, J., Prendergast, R., Walsh, D., Bryant, P., Levy, C. & Helliwell, J. R. (2012). *Acta Crystallogr D* **68**, 601-612.
- Thomas, B. R., Vekilov, P. G. & Rosenberger, F. (1996). *Acta Crystallogr D* **52**, 776-784.
- Tomasi, J., Mennucci, B. & Cammi, R. (2005). *Chem. Rev. (Washington, DC, U. S.)* **105**, 2999-3093.
- Tsekova, D. S., Williams, D. R. & Heng, J. Y. Y. (2012). *Chem. Eng. Sci.* **77**, 201-206.
- Tu, J. R., Miura, A., Yuyama, K., Masuhara, H. & Sugiyama, T. (2014). *Cryst. Growth Des.* **14**, 15-22.
- Vagin, A. & Teplyakov, A. (1997). *J. Appl. Crystallogr.* **30**, 1022-1025.
- Weiss, M. S., Palm, G. J. & Hilgenfeld, R. (2000). *Acta Crystallogr D* **56**, 952-958.
- Wilson, W. W. & DeLucas, L. J. (2014). *Acta Crystallographica Section F-Structural Biology Communications* **70**, 543-554.
- Winn, M. D., Ballard, C. C., Cowtan, K. D., Dodson, E. J., Emsley, P., Evans, P. R., Keegan, R. M., Krissinel, E. B., Leslie, A. G. W., McCoy, A., McNicholas, S. J., Murshudov, G. N., Pannu, N. S., Potterton, E. A., Powell, H. R., Read, R. J., Vagin, A. & Wilson, K. S. (2011). *Acta Crystallogr D* **67**, 235-242.
- Yeates, T. O. & Kent, S. B. H. (2012). *Annual Review of Biophysics*, Vol. 41, *Annual Review of Biophysics*, Vol 41, edited by D. C. Rees, pp. 41-61.